Supplementary Information

Controlling Stacking Order and Charge Transport in π-Stacks of Aromatic Molecules Based on Surface Assembly

[a]Department of Chemistry, Tokyo Tech., 2-12-1 W4-10 Ookayama, Meguro-ku, Tokyo 152-8511, Japan. E-mail: kiguti@chem.titech.ac.jp, fujii.s.af@m.titech.ac.jp

[b]Materials Research Center for Element Strategy, Tokyo Tech., 4259-S2-13 Nagatsuta-cho, Midori-ku, Yokohama 226-8503, Japan. E-mail: tada.t.ae@m.titech.ac.jp

[c]Department of Applied Chemistry, School of Engineering, The University of Tokyo, 7-3-1 Hongo, Bunkyo-ku, Tokyo 113-8656, Japan. E-mail: mfujita@appchem.t.u-tokyo.ac.jp

[d]Department of Material and Biological Chemistry, Faculty of Science, Yamagata University, 1-4-12 Kojirakawa-machi, Yamagata-shi, Yamagata 990-8560, Japan.

Madoka Iwane, [a] Tomofumi Tada,[b] Takafumi Osuga, [c] Takashi Murase, [d] Makoto Fujita,[c]* Tomoaki Nishino, [a] Manabu Kiguchi,[a]* Shintaro Fujii[a]**

Table of contents

1. Experimental details

Highly-oriented pyrolytic graphite (HOPG, ZYB grade, 12×12×2 mm) was purchased from Bruker Co.. A new surface of highly-oriented pyrolytic graphite (HOPG) was prepared by cleavage with adhesive tape before the block of graphite. The Au (111) substrate was prepared by the thermal evaporation of Au on mica. The tungsten (W) tip was prepared by electrochemical etching of W wires (diameter ≈ 0.3 mm; Nilaco) in 1M KOH aqueous solution. Sample molecules were deposited by immersion of the substrate into the corresponding 1.25 mM aqueous solutions for 2 hours. After deposition, the substrate was dried in an air flow.

Scanning tunneling microcopy (STM) imaging and current-voltage (*I*-*V*) characteristic measurement of single molecule was performed under the ambient conditions at room temperature using a commercially available STM system (Bruker, Nanoscope V). The current-voltage characteristic of a single molecular junction was measured as the following process. Firstly, the STM tip was approached toward the substrate till the tunneling current is above 70 nA at the sample bias voltage of 100 mV. Secondly, the tip was withdrawn by 10 nm at a speed of 1.07 Hz to make a nanogap between the STM tip and substrate, forming the molecular junction during current monitoring at a fixed bias voltage of 100 mV. Thirdly, the tip position was fixed and one *I*-*V* curve was recorded by scanning the bias voltage from 100 to 1500, –1500 mV, and back to 100 mV at constant tip-sample separation. Finally, the junction was broken by pulling the STM tip away from the substrate.

2. STM images of the sample surface

2-1. HOPG

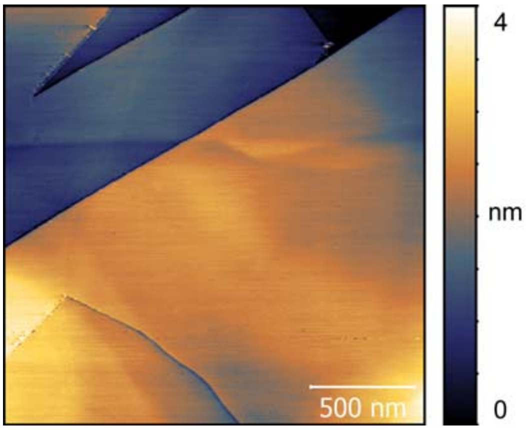

Figure S1. STM images of the HOPG surface (tunneling current = 250 pA, sample bias voltage = 1.1 V).

2-2. Homo stack on Au(111)

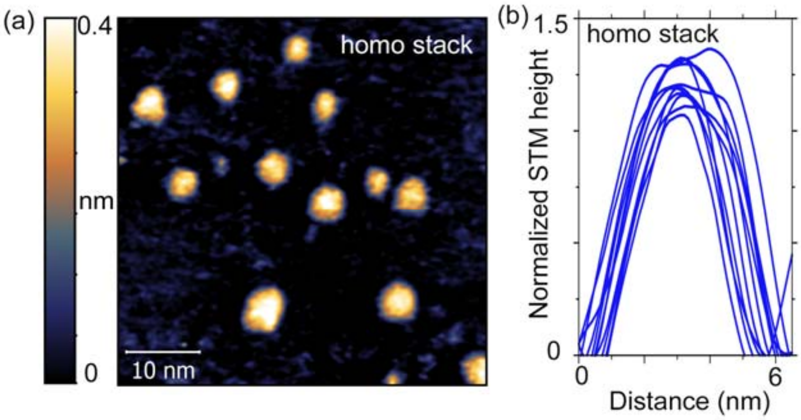

Figure S2. (a) STM images of the homo stack, **1**·(**2**·**2**), on a Au(111) surface (imaging area = 40×40 nm^2, I_t = 200 pA, V_s = 0.5 V). (b) Cross-sectional profiles of the isolated homo stack observed in (a). The variation in the STM intensity was low (<30%), which suggests the epitaxial adsorption of the π-stack on the Au(111) surface.

2-3. Annealing effect of the hetero stack on Au(111)

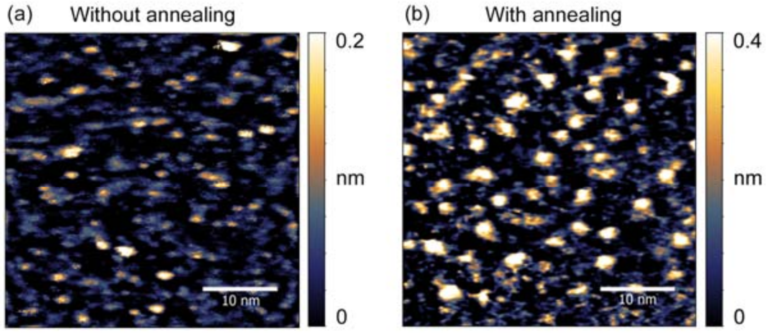

Figure S3. STM images of the hetero stack, **1·(2·3)**, on Au(111) (a) without and (b) with annealing (tunneling current = 200 pA, sample bias voltage = 1.0 V). The annealing was performed at 90 °C for 2 hours in the molecular solution.

To check the kinetic trap effect for the hetero-π-stack **1·(2·3)** on Au(111) (Figure 2c), the hetero-π-stack molecules were adsorbed on the surface at elevated temperature. The annealing at 90 °C led to more uniform contrast of the hetero-π-stacks molecules in STM images, suggesting that one of the molecular orientations (i.e., **1'**·(**A**·**D**)·**1''**/**Au**) could be predominantly formed at the elevated temperature.

2-4. Homo stack on HOPG

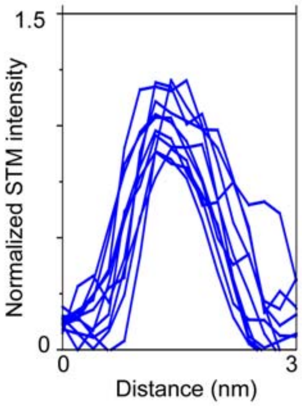

Figure S4. Cross-sectional profiles of the isolated homo stack observed in Figure 1b (See main text). The variation in the STM intensity was low (<30%), which suggests the epitaxial adsorption of the π-stack on the HOPG surface

3. Calculated single-molecule conductance from *I-V* curves

Intrinsic charge transport properties of single-molecule junctions were measured by approaching the STM tip to the individual molecules on the HOPG or Au(111) substrates. To ensure that the STM tip was made contact with the individual molecules on the substrates to form the single-molecule junctions, the STM tip (*i.e.*, top electrode) was approached to the individual molecules until an electronic contact with conductance of 10^{-2} G_0 (100 nA at the sample bias voltage of 0.1 V) was established. In the previous single-molecule transport studies on the homo and hetero stacks sandwiched by Au electrodes, the single-molecule conductance values have been determined by 10^{-3}~10^{-2} G_0 ($G_0 = 2e^2/h$). [1] Therefore, in the present study, the STM tip was approached to the individual molecules on the HOPG or Au(111) substrates until the conductance (current) exceeded 10^{-2} G_0 (100 nA at the sample bias voltage of 0.1 V) to make single-molecule junction-structures between the STM tip and the substrates. In the present study, Figure S5 shows conductance histograms of the molecular junctions that were calculated from *I-V* curves in Figure 3 at the low and high bias voltages. At the low bias voltage of 0.1 V, the histograms feature single-molecule conductance of $< 10^{-3}$ G_0 (Figure S5(a)(c)), which assures that the electronic contact of 10^{-2} G_0 (100 nA at the sample bias voltage of 0.1 V) is appropriate for the junction-formation.

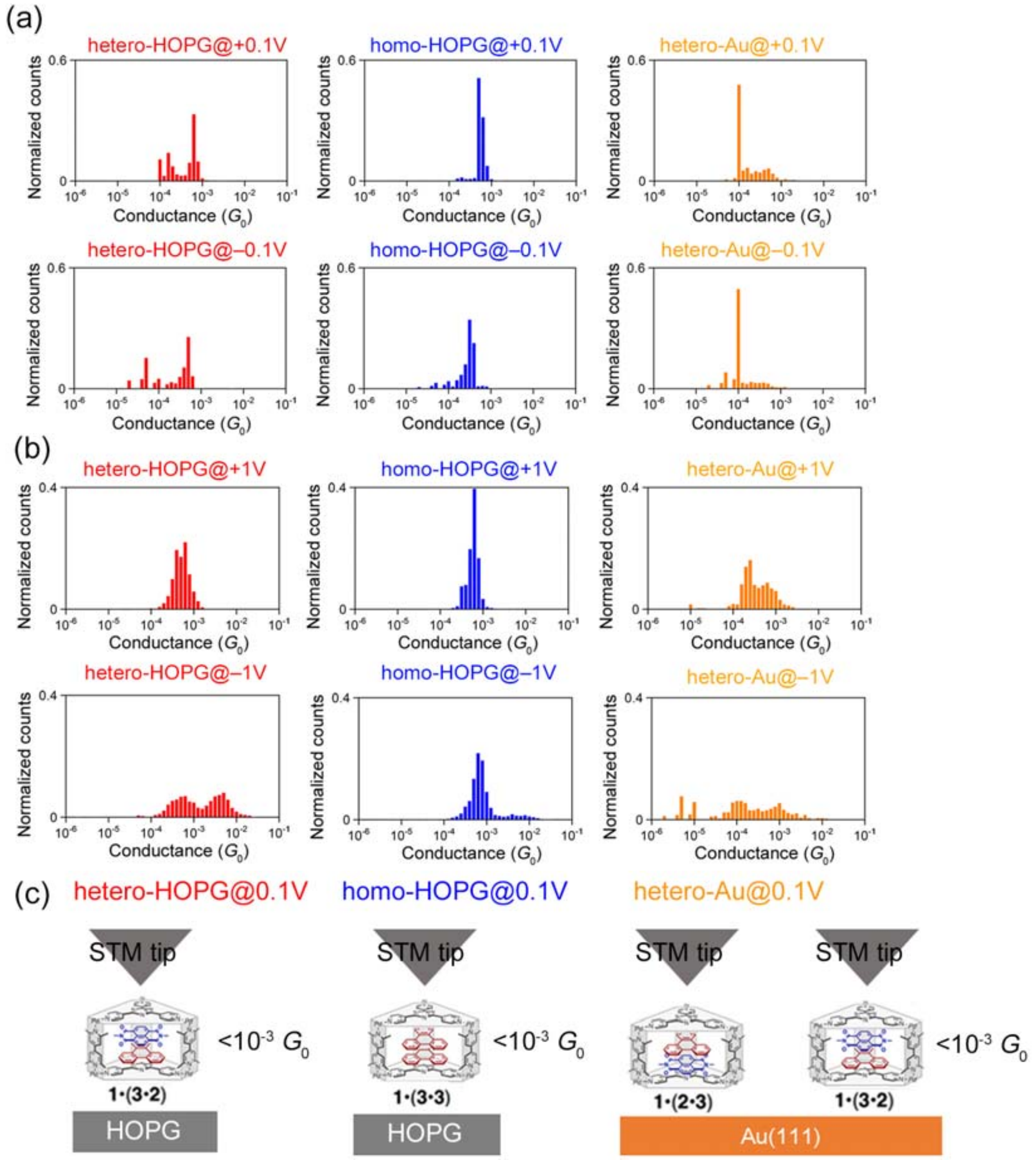

Figure S5. (a,b) Histograms of calculated molecular conductance from *I-V* curves in Fig. 3 at the low bias voltage of ±0.1 V and the high bias voltage ±1 V. (c) Schematic illustration of junction structures and molecular conductance values found in (a).

4. **Current-voltage characteristic and rectification histograms of molecular junctions**

Figure S6 shows examples of *I-V* curves for the hetero stack on HOPG (hetero-HOPG), the homo stack on HOPG (homo-HOPG) and the hetero stack on Au(111) (hetero-Au). The asymmetric I-V curve was obtained for hetero-HOPG, while symmetric *I-V* curves were observed for homo-HOPG and hetero-Au. It is noted that asymmetric curves are observed for hetero-Au, but the difference in current between positive and negative bias voltage is much smaller than that for hetero-HOPG, and the polarity where larger current is observed varies with the sample, and thus, the distribution seems symmetric for hetero-Au.

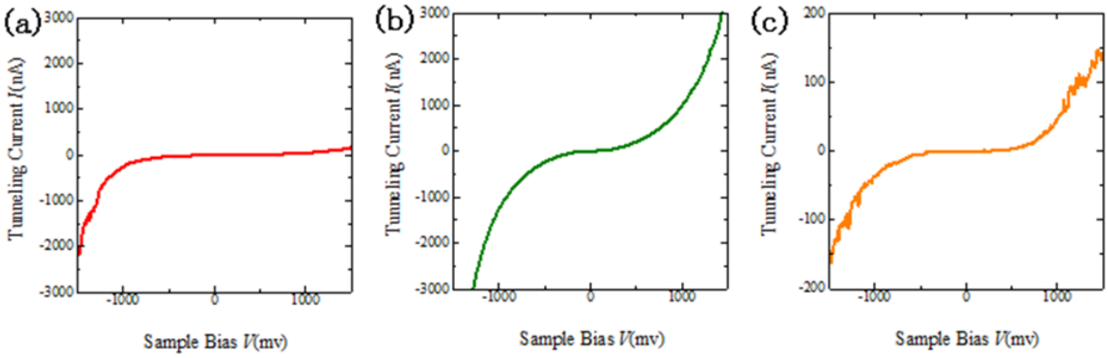

Figure S6. Example of I-V curves for (a) hetero-HOPG (b) homo-HOPG (c) hetero-Au.

Figure S7 shows 2D histograms of the I−V characteristics and rectification histogram of the samples of hetero-HOPG, homo-HOPG, hetero-Au, and HOPG. *I-V* measurement was also performed for clean HOPG samples without the molecular deposition.

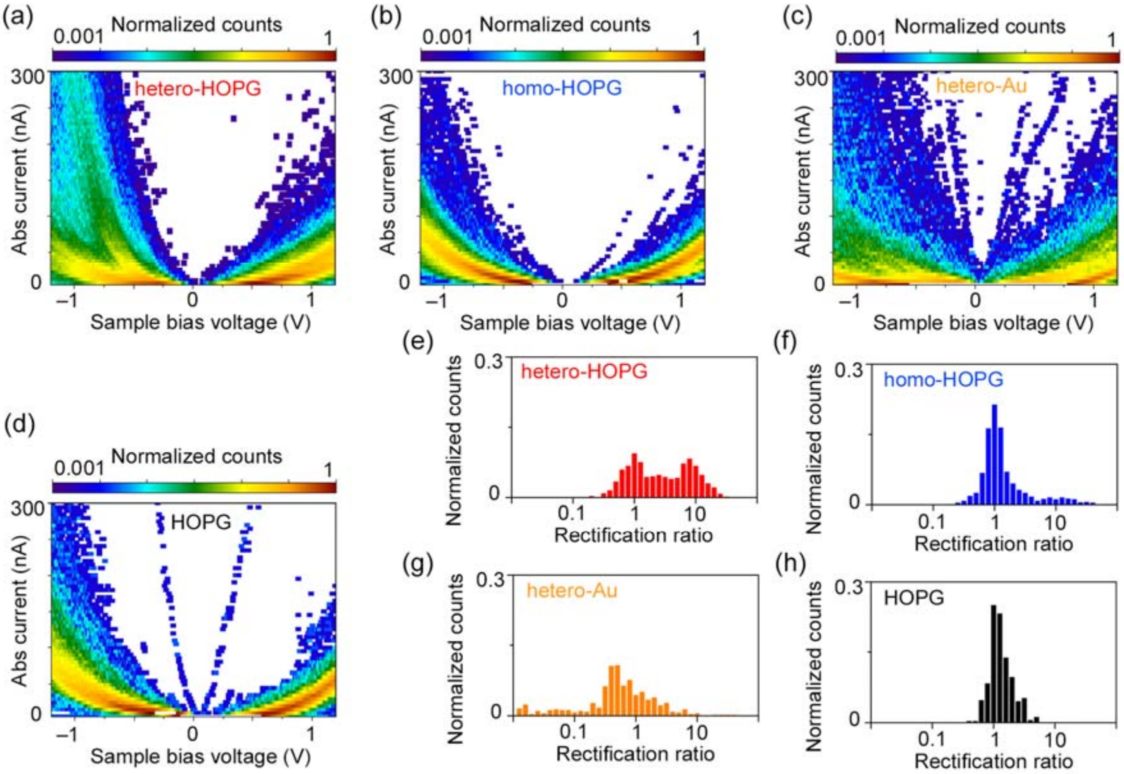

Figure S7. 2D histograms of the *I*−*V* curves for a) hetero-HOPG, b) homo-HOPG, c) hetero-Au, and d) HOPG, which are, respectively, constructed from 1612, 1242, 590, and 445 I-V curves. Normalized counts are plotted logarithmically. Histograms of the rectification ratio of mean current at the negative and positive bias voltage of 1.2 V for e) hetero-HOPG f) homo-HOPG g) hetero-Au and h) HOPG.

5. Theoretical calculations

5-1. Computational Conditions

All vdW-DFT calculations were carried out using Vienna Ab initio Simulation Package (VASP 5.2), and the generalized gradient approximation (GGA) with the Perdew-Burke-Ernzerhof (PBE) type was adopted as the exchange-correlation functional in DFT. We used the cutoff energy of 500 eV and Gamma point approximation as the k-point sampling. DFT-D2 method by Grimm was adopted for vdW interactions; the C6 and R0 parameters adopted in this study are respectively 40.62 Jnm^6/mol and 1.771 Å for Au, 24.670 and 1.639 for Pd, 1.750 and 1.452 for C, 1.230 and 1.397 for N, 0.700 and 1.342 for O, and 0.140 and 1.001 for H.

5-2. Adsorption Structures

As described in the calculation part in the main text, we adopted an expression **1’·(D·A)·1’/Sub** instead of **1’·(2·3)·1’/Sub** to represent a stacking sequence of π-stack molecules, where **Sub** indicates the substrate HOPG or Au. We optimized five adsorption configurations for **1’·(D·A)·1’**/HOPG, five configurations for **1’·(A·D)·1’**/HOPG, eleven configurations for **1’·(D·A)·1’**/Au(111), and eleven configurations for **1’·(A·D)·1’**/Au(111). The calculated total energies of the configurations are listed in Table S1, in which “site index” indicates the site categories of adsorption configurations. For HOPG substrate, the site indices are given as AA or AB together with a number. AA corresponds to an A-A stack (i.e., the perfect match in the stacking structure between the carbon of HOPG and molecule **1’**) and AB corresponds to an A-B stacking structure for those. The numbers attached with AA/AB indicate the rotational angle of molecule **1’** with respect to the AA/AB non-rotated configuration. The optimized structures for **1’·(D·A)·1’**/HOPG and **1’·(A·D)·1’**/HOPG are shown in Figures S8 and S9. For Au(111) substrate, the site indices are given as Bri, Hcp, Fcc, or Top together with a number, where Bri, Hcp, Fcc, and Top respectively correspond to the bridge, hcp, fcc, and top adsorption positions for the center of molecule **1’** on Au(111). The numbers attached with those indices are the rotational angle of molecule **1’** with respect to the non-rotated configurations. The optimized structures for **1’·(D·A)·1’**/Au(111) and **1’·(A·D)·1’**/Au(111) are shown in Figures S10 and S11.

According to the calculated total energies, we found **1’**·(**A**·**D**)·**1’/Ele** is more stable than **1’**·(**D**·**A**)·**1’/Ele**. Table S1 lists the appearance probability of each configuration by using the Boltzmann factor at room temperature. According to the probability data, the **1’·(A·D)·1’/Ele** orientation appears with higher probability than **1’**·(**D**·**A**)·**1’/Ele** for both Au and HOPG electrodes. The calculated high probability of the **1’·(A·D)·1’/ HOPG** agrees with the experimental observations (Figure 2a and Figures 3a,d). On the other hand, the calculation suggests high probability only for the **1’·(A·D)·1’/Au** orientation on Au, which disagrees with the experiments where both orientations (i.e., **1’·(A·D)·1’/Au and 1’·(D·A)·1’/Au**) were observed (Figure 2c and Figures 3c,f). The calculated probability based on the relative energetic stability for the molecular orientations on the electrodes failed to explain the experimental observations. Therefore, we performed more quantitative calculations using realistic models.

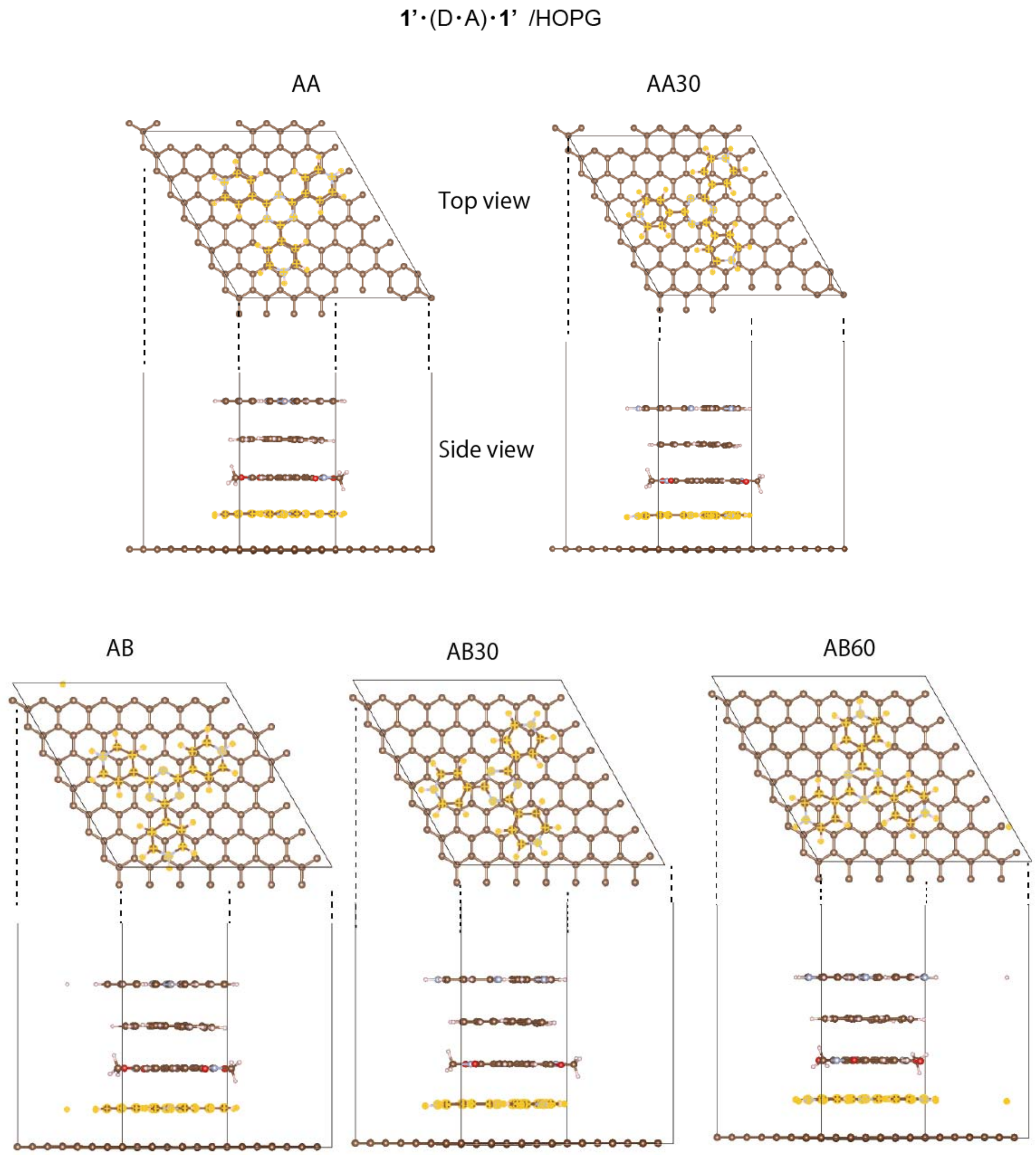

Figure S8. Optimized adsorption structures of **1'·(D·A)·1'**/HOPG. For the top views, molecule **1'** (hatched in the side views) and substrate are depicted to recognize the relative positon of π-stack molecules.

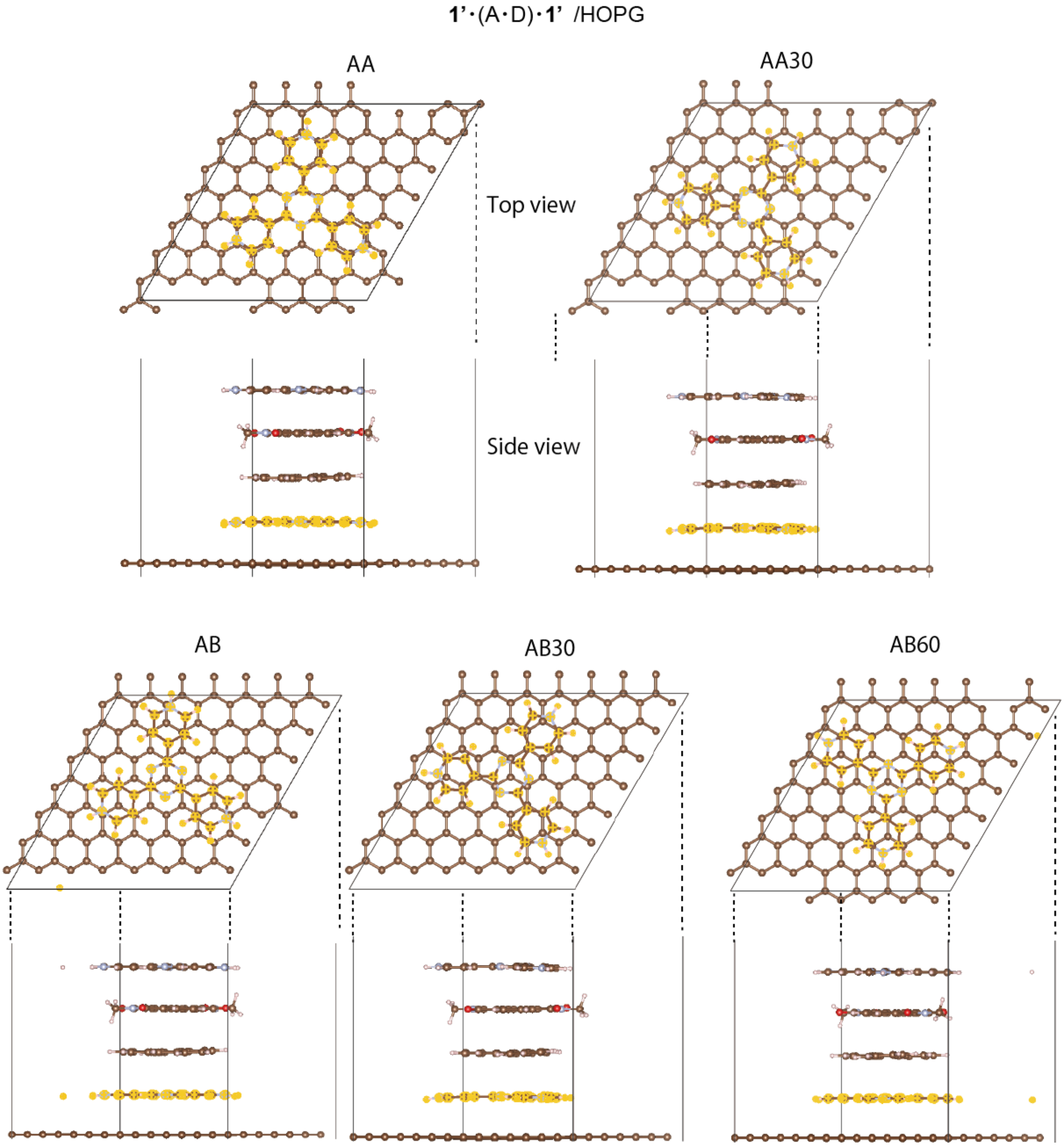

Figure S9. Optimized adsorption structures of **1’·(A·D)·1’**/HOPG. For the top views, molecule **1’** (hatched in the side views) and substrate are depicted to recognize the relative positon of π-stack molecules.

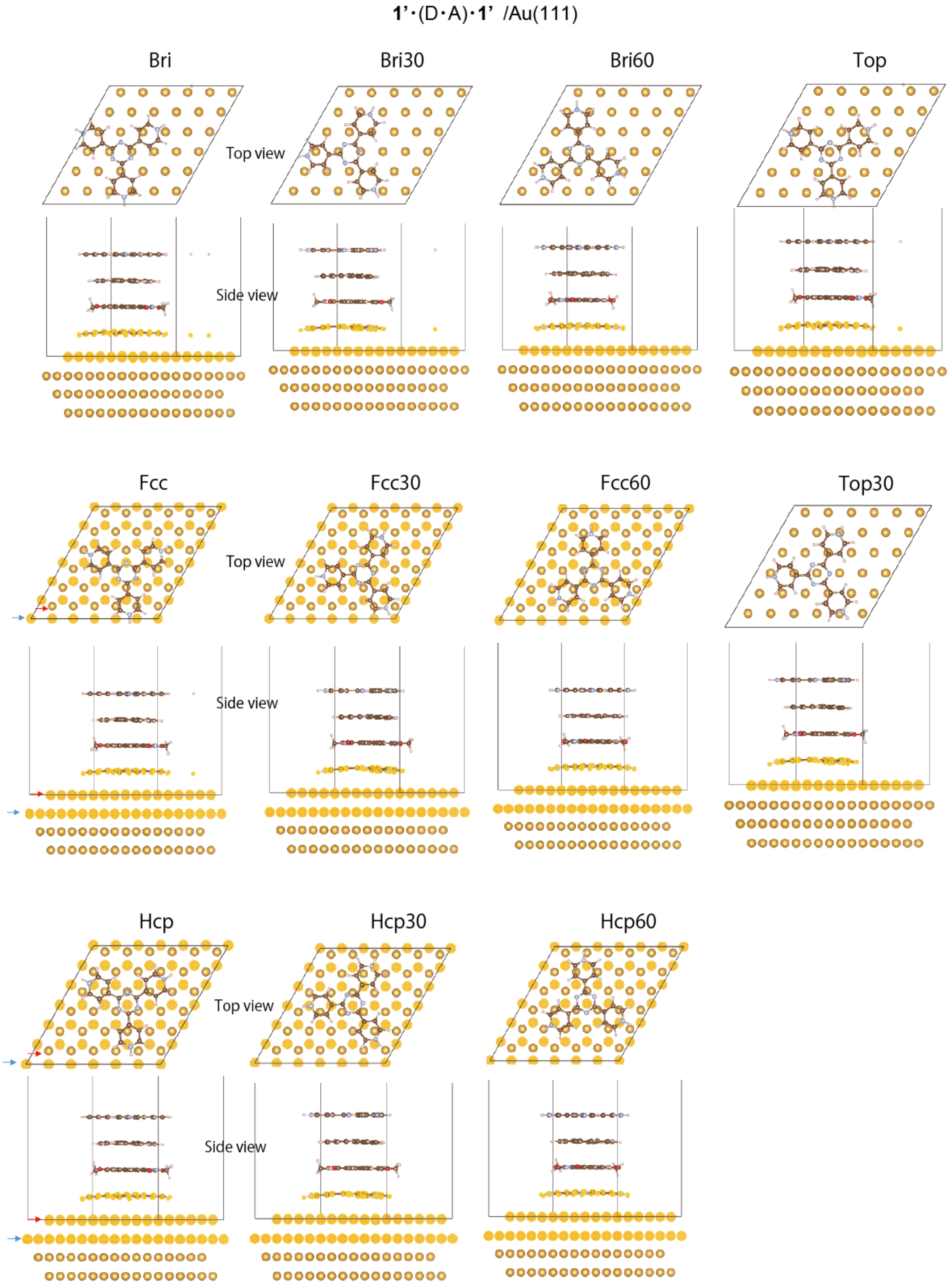

Figure S10. Optimized adsorption structures of **1'·(D·A)·1'**/Au(111). For the top views, molecule **1'** (hatched in the side views) and the first or first-and-second layers of substrate are depicted to recognize the relative positon of π-stack molecules.

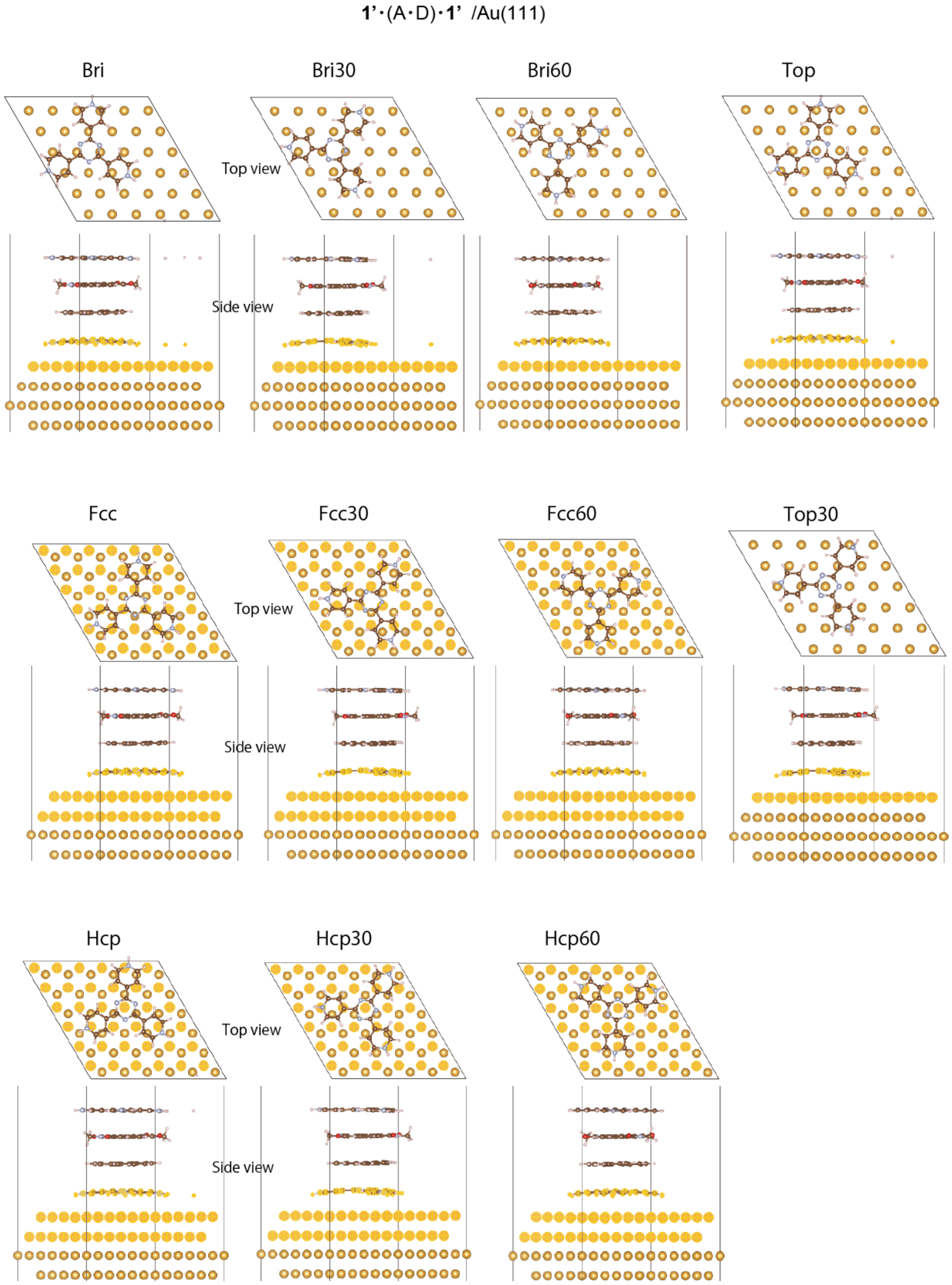

Figure S11. Optimized adsorption structures of **1’·(A·D)·1’**/Au(111). For the top views, molecule **1’** (hatched in the side views) and the first or first-and-second layers of substrate are depicted to recognize the relative positon of π-stack molecules.

Table S1. Calculated total energies (Tot E), adsorption energies (AE), and appearance probability (Prob). The relative Tot E are the shifted total energy with respect to the most stable one. Adsorption energy (AE) is defined as the subtracted total energy of a π-stack on substrate from the total energies of isolated π-stack and isolated substrate; the negative number of AE means stabilization by the adsorption of π-stack on substrates.

Sub	Configuration	Site index	Relative Tot E (eV)	AE (eV)	Prob.
HOPG	**1’·(D·A)·1’**/Sub.	AA	0.264	−1.784	0.0000
		AA30	0.130	−1.917	0.0050
		AB	0.213	−1.835	0.0002
		AB30	0.094	−1.954	0.0208
		AB60	0.164	−1.884	0.0014
	1’·(A·D)·1’/Sub.	AA	0.185	−1.862	0.0006
		AA30	0.041	−2.006	0.1632
		AB	0.161	−1.887	0.0015
		AB30	**0.000**	**−2.047**	**0.8035**
		AB60	0.137	−1.910	0.0038
Au(111)	**1’·(D·A)·1’**/Sub.	Bri	0.334	−5.584	0.0000
		Bri30	0.218	−5.699	0.0001
		Bri60	0.330	−5.588	0.0000
		Hcp	0.306	−5.612	0.0000
		Hcp30	0.230	−5.688	0.0001
		Hcp60	0.311	−5.607	0.0000
		Fcc	0.343	−5.575	0.0000
		Fcc30	0.182	−5.736	0.0004
		Fcc60	0.332	−5.586	0.0000
		Top	0.374	−5.543	0.0000
		Top30	0.283	−5.635	0.0000
	1’·(A·D)·1’/Sub.	Bri	0.122	−5.796	0.0042
		Bri30	0.009	−5.908	0.3376
		Bri60	0.122	−5.796	0.0042
		Hcp	0.109	−5.809	0.0069
		Hcp30	**0.000**	**−5.918**	**0.4889**
		Hcp60	0.114	−5.803	0.0056
		Fcc	0.143	−5.775	0.0019
		Fcc30	0.038	−5.880	0.1125
		Fcc60	0.132	−5.786	0.0029
		Top	0.188	−5.730	0.0003
		Top30	0.068	−5.850	0.0340

5-3. More realistic π-Stack models with Pd-complex and NO_3^-

π-Stack molecules attached with Pd-complex cations and counter anions NO_3^-

To represent the adsorption energies more quantitatively than those calculated using the only-π models, Pd-complexes and counter anions (NO_3^-) are attached to the bottom π-molecule (the extended π by Pd-complexes with NO_3^- is abbreviated as **1’’**; see Figure S12), and the adsorption energies of **1’**·(**A**·**D**)·**1’’/Ele** and **1’**·(**D**·**A**)·**1’’/Ele**, where **Ele** indicates HOPG or Au(111), are recalculated using the same conditions of DFT calculations described in **5-1**. As for the relative site-positions of the π-molecules on the substrates, we select the most stable sites (i.e., AB30 for both **1’**·(**A**·**D**)·**1’’/HOPG** and **1’**·(**D**·**A**)·**1’’/HOPG,** Hcp30 for **1’**·(**A**·**D**)·**1’’**/**Au(111)** , and Fcc30 for **1’**·(**D**·**A**)·**1’’**/**Au(111)**) as the initial adsorption sites.

Let us first explain the computational results on **1’**·(**A**·**D**)·**1’’/HOPG** and **1’**·(**D**·**A**)·**1’’/HOPG**. The full-relaxed structure of **1’**·(**A**·**D**)·**1’’/HOPG** is shown in Figure S13, and the calculated adsorption energies of **1’**·(**A**·**D**)·**1’’/HOPG** and **1’**·(**D**·**A**)·**1’’/HOPG** are respectively −1.299 and −0.959 eV, which show large upward shifts from the only-π model; −2.047 and −1.954 eV respectively for **1’**·(**A**·**D**)·**1’/HOPG** and **1’**·(**D**·**A**)·**1’/HOPG,** as listed in Table S1. However, the recalculated adsorption energies are still large with the negative signs in both orientations. Looking at the full-relaxed structures carefully, we expect that the full-relaxation might lead to too much relaxed structures in comparison with a realistic situation for the π-stack molecules on the HOPG substrate. The reasons for the observation are i) the carbon sheet in Figure S13 shows a highly rippled structure, although the top carbon sheet of a realistic HOPG substrate is much more structurally restricted because of the attractive interactions with underlying carbon sheets of HOPG, and ii) the Pd-complex groups rotate almost freely to reduce the steric hindrance with the carbon sheet, although the structure of Pd-complex groups in a realistic situation are almost fixed by the presence of the pillar π-molecules (See Figure S12(a)) . That is, the calculated adsorption energies with the full-relaxation still include artificial effects, and thus partial fixation of the structures are required to bring the computation condition closer to the experimental situation. We introduce the partial fixation of structures in a stepwise manner; i) the single carbon sheet is fixed to the planer one, ii) the upper nitrogen atoms of the Pd complex (indicated with a blue arrow in Figure S12 (a)) are fixed to the positions of the isolated structure, and iii) the upper carbon atoms in the Pd complex (indicated with a red arrow in Figure S12 (a)) are fixed to the positions of the isolated structure. The condition i) corresponds to the suppression of the ripple structure of carbon sheet, and conditions ii) and iii) suppress the rotation of Pd-complex. In the partially fixed calculations, we also fix the height of Pd atoms from the carbon sheet to that obtained in the full relaxation.

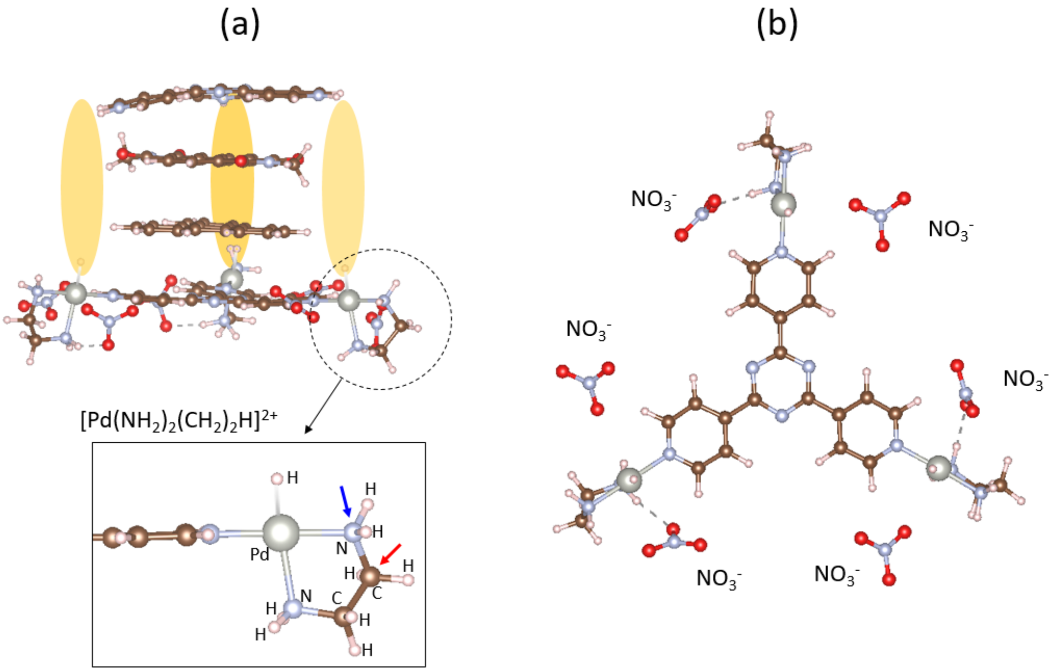

Figure S12. Optimized structure of the isolated **1’·(A·D)·1”** molecule; (a) a side view and (b) top view. In the side view, the yellow shaded regions correspond to the positions of π-pillar molecules (see Figure 1 in the main text), which are replaced with hydrogen atoms in this model. In the top view, the π-molecules which are not bonded to Pd complexes are omitted in the picture.

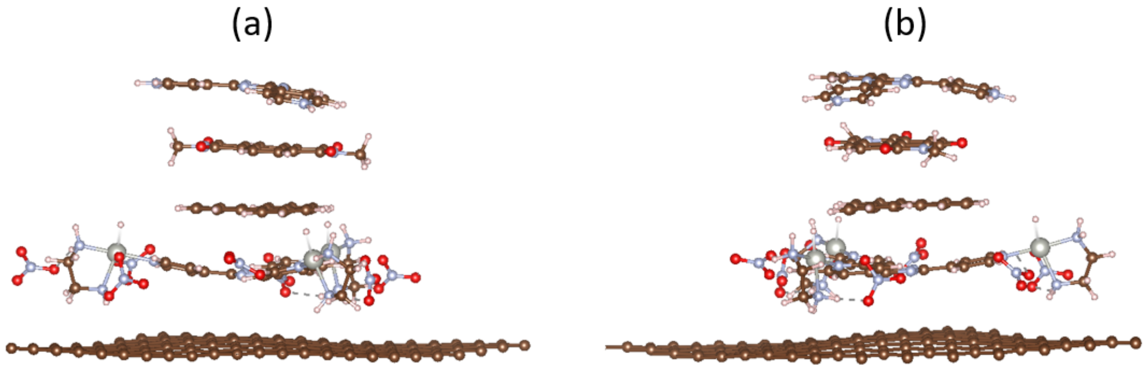

Figure S13. Full-relaxed structure of **1’·(A·D)·1”/HOPG** molecule; (a) side view I, and (b) side view II.

Figure S14 shows the calculated adsorption energies of **1’·(A·D)·1’’/HOPG** and **1’·(D·A)·1’’/HOPG** in the partially fixed relaxation, together with the results using only-π models. Although the partially fixed condition i) (P-fixed i) in Figure S14) leads to a little reduced adsorption energies in comparison with the full-relaxations, those numbers are still negative. However, we find the partially fixed conditions i,ii) and i,ii,iii) result in the drastically different results in adsorption energies: In conditions i,ii), the adsorption energies of **1’·(A·D)·1’’/HOPG** and **1’·(D·A)·1’’/HOPG** are respectively −0.314 and −0.008 eV, and in conditions i,ii,iii), the adsorption energies of **1’·(A·D)·1’’/HOPG** and **1’·(D·A)·1’’/HOPG** are respectively −0.078 and +0.237 eV. Since the partially fixed conditions i,ii) and i,ii,iii) can be regarded as the closest conditions in the present partially fixed conditions, these results indicate the **1’·(D·A)·1’’/HOPG** adsorption cannot be expected to occur in a realistic situation. We also calculated the adsorption energies for the Au(111) substrate, and the adsorption energies of **1’·(A·D)·1’’/Au(111)** and **1’·(D·A)·1’’/Au(111)** in the full-relaxation are calculated to be −10.631 and −10.329, respectively. Although we don’t introduce the partially fixed relaxations for Au(111) substrate, we can conclude from the very large adsorption energies that both **1’·(A·D)·1’’/Au(111)** and **1’·(D·A)·1’’/Au(111)** adsorptions still can be expected to occur with a slightly larger stabilization in **1’·(A·D)·1’’/Au(111)** than **1’·(D·A)·1’’/Au(111)**, like in the only-π models on Au(111) substrate.

We also confirm that the interactions (i.e., orbital hybridizations) are still remain in the **1’·(A·D)·1’’/Ele** and **1’·(D·A)·1’’/Ele** by looking at the calculated density of states. Figure S15 shows the density of states and electron density distributions of **1’·(A·D)·1’’/HOPG** in the four energy regions, and the orbital hybridizations especially between HOPG and bottom π-molecule, are clearly confirmed. The situation is qualitatively similar to that obtained in only-π models. That is, to investigate the qualitative electronic states of these adsorption systems, simplified models in which π-stack molecules are only included in the calculations are still useful.

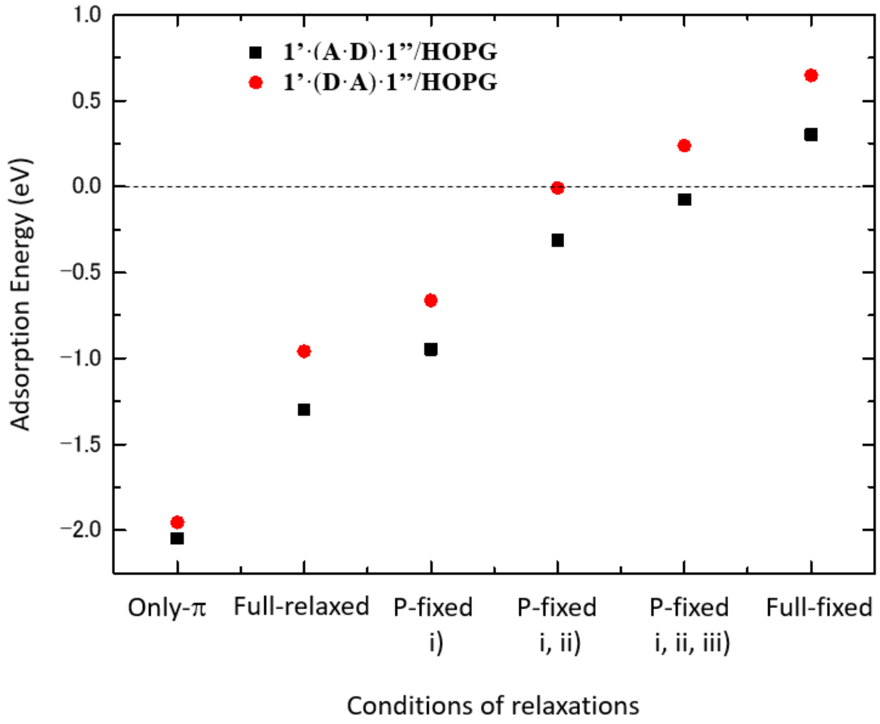

Figure S14. Calculated adsorption energies in different types of relaxations. P-fixed indicates the partially fixed calculations, and the indices i, ii, and iii indicate the partially fixed conditions.

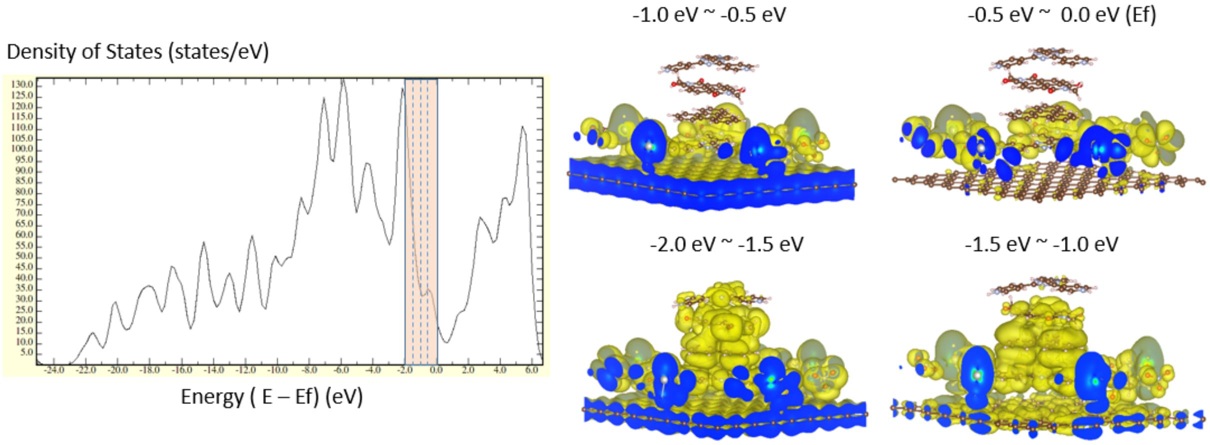

Figure S15. Calculated density of states (left) and electron density distributions (right) of **1'·(A·D)·1''/HOPG**.

5-4. Calculated Bader charges on each unit

In the simplified π-stack model, the calculated Bader charges of HOPG and molecule **1’** directly attached on HOPG are respectively −0.51 and +0.60, and those on Au(111) and molecule **1’** on Au(111) are respectively −1.46 and +1.25. The large charge transfer in the Au substrate corresponds to the stronger adsorption of the π-stack molecule on the Au substrate than that on HOPG. The large difference on the amount of charge transfer between both substrates is probably coming from the difference of the density of states (DOS) at the Fermi level in the substrates; Au(111) shows much larger DOS than HOPG Dirac cone.

5-5. Electrostatic energy

We evaluated the energy difference between the both configurations in the electrostatic point of view. Using the information that the **A**-Substrate distance changes 3.2 Å when **1'·(A·D)·1'**/Substrate is changed to **1'·(D·A)·1'**/Substrate, and that the charges on **A** and Substrate are both −0.5 (*i.e.*, HOPG case), the energy change from **1'·(A·D)·1'**/Substrate to **1'·(D·A)·1'**/Substrate is about +0.1 eV. This corresponds well to DFT results on HOPG. In addition, when we assume the charges on A and Substrate are both −1.0, the energy change from **1'·(A·D)·1'**/Substrate to **1'·(D·A)·1'**/Substrate is about +0.4 eV, roughly corresponding to DFT results on Au(111). That is, simple electrostatic interactions can be the reason for the preferred orientation.

6. Reference

[1] S. Fujii, T. Tada, Y. Komoto, T. Osuga, T. Murase, M. Fujita, and M. Kiguchi, *J. Am. Chem. Soc.,* 2015, **137**, 5939-5947.